

# ROBUST AND TREND-FOLLOWING STUDENT'S T-KALMAN SMOOTHERS

ALEKSANDR Y. ARAVKIN\*, JAMES V. BURKE†, AND GIANLUIGI PILLONETTO ‡

**Abstract.** We present a Kalman smoothing framework based on modeling errors using the heavy tailed Student's t distribution, along with algorithms, convergence theory, open-source general implementation, and several important applications. The computational effort per iteration grows linearly with the length of the time series, and all smoothers allow nonlinear process and measurement models.

Robust smoothers form an important subclass of smoothers within this framework. These smoothers work in situations where measurements are highly contaminated by noise or include data unexplained by the forward model. Highly robust smoothers are developed by modeling *measurement* errors using the Student's t distribution, and outperform the recently proposed  $\ell_1$ -Laplace smoother in extreme situations with data containing 20% or more outliers.

A second special application we consider in detail allows tracking sudden changes in the state. It is developed by modeling *process* noise using the Student's t distribution, and the resulting smoother can track sudden changes in the state.

These features can be used separately or in tandem, and we present a general smoother algorithm and open source implementation, together with convergence analysis that covers a wide range of smoothers. A key ingredient of our approach is a technique to deal with the non-convexity of the Student's t loss function. Numerical results for linear and nonlinear models illustrate the performance of the new smoothers for robust and tracking applications, as well as for mixed problems that have both types of features.

**1. Introduction.** The Kalman filter is an efficient recursive algorithm for estimating the state of a dynamic system [18]. Traditional formulations are based on  $\ell_2$  penalties on model deviations, and are optimal under assumptions of linear dynamics and Gaussian noise. Kalman filters are used in a wide array of applications including navigation, medical technologies, and econometrics [11, 25, 29]. Many of these problems are nonlinear, and may require smoothing over past data in both online and offline applications to significantly improve estimation performance [15].

This paper focuses on two important areas in Kalman smoothing: robustness with respect to outliers in measurement data, and improved tracking of quickly changing system dynamics. Robust filters and smoothers have been a topic of significant interest since the 1970's, e.g. see [24]. Recent efforts have focused on building smoothers that are robust to outliers in the data [2, 3, 14], using convex loss functions such as  $\ell_1$ , Huber or Vapnik, in place of the  $\ell_2$  penalty [17].

There have also been recent efforts to design smoothers able to better track fast system dynamics, e.g. jumps in the state values. A contribution can be found in [21] where the Laplace distribution, rather than the Gaussian, is used to model transition noise. This introduces an  $\ell_1$  penalty on the state evolution in time, resulting in an estimator interpretable as a dynamic version of the well known LASSO procedure [26].

For known dynamics, all of the smoothers mentioned above can be derived by modeling the process and the measurement noise using log-concave densities, taking the form

$$\mathbf{p}(\cdot) \propto \exp(-\rho(\cdot)), \quad \rho \text{ convex} . \quad (1.1)$$

\*IBM T.J. Watson Research Center, Yorktown Heights, NY, 10598 (saravkin@us.ibm.com).

†Mathematics Dept., University of Washington, Seattle, WA 98195 (burke@math.washington.edu).

‡Control and Dynamic Systems Department of Information Engineering at the University of Padova, Padova, Italy (giapi@dei.unipd.it)

November 27, 2024

Formulations exploiting (1.1) are nearly ubiquitous, in part because they correspond to convex optimization problems in the linear case. However, in order to model a regime with large outliers or sudden jumps in the state, we want to look beyond (1.1) and allow heavy-tailed densities, i.e. distributions whose tails are not exponentially bounded. All such distributions necessarily have non-convex loss functions [6, Theorem 2.1].

Several interesting candidates are possible, but in this contribution we focus on the Student’s t-distribution for its convenient properties in the context of the applications we consider. The Student’s t-distribution was successfully applied to a variety of robust inference applications in [19], and is closely related to re-descending influence functions [16].

In this work, we propose a smoothing framework for several applications, including robust and trend smoothing. The T-Robust smoother is derived from a dynamic system with *output noise* modeled by the Student’s t-distribution. This is a further robustification of the estimator proposed in [2], which uses the Laplace density. The re-descending influence function of the Student’s t guarantees that outliers in the measurements have less of an effect on the smoothed estimate than any convex loss function. In practice, the T-Robust smoother performs better than [2] for cases with a high proportion of outliers. The T-Trend smoother is similarly derived starting from a dynamic system with *transition noise* modeled by the Student’s t-distribution. This allows T-Trend to better track sudden changes in the state. One may consider using both aspects simultaneously; in addition, practitioners need the ability to distinguish between different measurements based on prior information of measurement fidelity, and between different states based on prior knowledge of trend stability.

In the context of Kalman filtering/smoothing, the idea of using Student’s t-distributions to model the system noise for robust and tracking applications was first proposed in [13]. However, our work differs from that approach in some important aspects. First, our analysis includes nonlinear measurement and process models. Second, we provide a novel approach to overcome the non-convexity of the Student’s t-loss function. Third, the approach we propose can be used to solve *any* smoothing problem that uses Student’s t modeling for any process or measurement components.

The basic approach differs significantly from the one proposed in [13]. [13] proposes using the random information matrix (i.e. full Hessian) when possible, or its expectation (Fisher information) when the Hessian is indefinite. Instead, we propose a modified Gauss-Newton method which builds information about the curvature of the Student’s t-log likelihood into the Hessian approximation, and is guaranteed to be positive definite. As we show in Section 5, the new approach is provably convergent, and unlike the approach in [13] uses information about the relative sizes of the residuals in computing descent directions. These differences make it more stable than methods using random information, and more efficient than methods using Fisher information. The major computational tradeoff in using non-convex penalties is that the loss function in the convex case is used directly [2], i.e. is not approximated, whereas in the nonconvex case, the loss function must be iteratively approximated with a local convex approximation. This requires a fundamental extension of the convergence analysis.

A conference proceeding previewing this paper appears in [5]. In the current work, we present a general smoothing framework that includes the two smoothers presented in [5] as special cases, together with a generalized convergence theory that covers the entire range of smoothers under discussion. We also provide an open-source implementation of the general algorithm [1], with a simple interface that enables

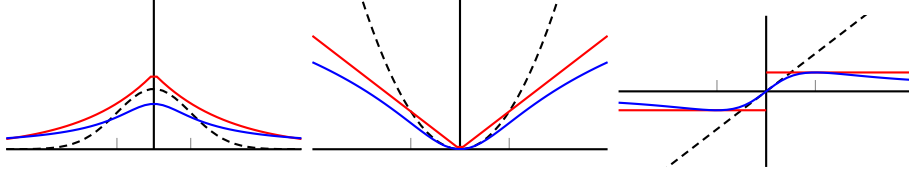


FIG. 2.1. *Gaussian, Laplace, and Student's t Densities, Corresponding Negative Log Likelihoods, and Influence Functions.*

the user to customize which residual or innovation components to model using the Student's t penalty. Using this implementation, we present an expanded experimental section, and new experiments that show how robust and trend smoothing can be done simultaneously. Finally, we apply the smoothers to real data.

The paper is organized as follows. In Section 2, we introduce the multivariate Student's t-distribution, review its advantages for error modeling over log-concave distributions, and introduce the dynamic model class of interest for Kalman smoothing. In Section 3, we describe a statistical modeling framework, where we can use Student's t to model any process or measurement residual components. We describe all objectives that can arise this way, and provide a comprehensive method for obtaining approximate second order information for these objectives. In Section 4, we provide details for three important special smoothers: T-Robust (robust against large measurement noise), T-Trend (able to follow sharp changes in the state), and the Double-T smoother (incorporates both aspects). In Section 5, we present the algorithm and a convergence theory for the entire framework, which also extends the convergence theory developed in [2]. In Section 6, we present numerical experiments that illustrate the behavior of all three special smoothers, include illustrations of linear and nonlinear models, and results for real and simulated data. We end the paper with concluding remarks.

**2. Error Modeling with Student's t.** For a vector  $u \in \mathbb{R}^n$  and any positive definite matrix  $M \in \mathbb{R}^{n \times n}$ , let  $\|u\|_M := \sqrt{u^T M u}$ . We use the following generalization of the Student's t-distribution:

$$\mathbf{p}(v_k | \mu) = \frac{\Gamma(\frac{s+m}{2})}{\Gamma(\frac{s}{2}) \det[\pi s R]^{1/2}} \left( 1 + \frac{\|v_k - \mu\|_{R^{-1}}^2}{s} \right)^{-\frac{(s+m)}{2}} \quad (2.1)$$

where  $\mu$  is the mean,  $s$  is the degrees of freedom,  $m$  is the dimension of the vector  $v_k$ , and  $R$  is a positive definite matrix. A comparison of this distribution with the Gaussian and Laplacian distribution appears in Figure 2. Note that the Student's t-distribution has much heavier tails than the others, and that its influence function is re-descending, see [20] for a discussion of influence functions. This means that as we pull a measurement further and further away, its 'influence' decreases to 0, so it is eventually ignored by the model. Note also that the  $\ell_1$ -Laplace is peaked at 0, while the Student's t-distribution is not, and so a Student's t-fit will not in general drive residuals to be exactly 0.

Before we proceed with the Kalman smoothing application, we review a result from [6], illustrating the fundamental modeling advantages of heavy tailed distributions:

**THEOREM 2.1.** *Consider any scalar density  $p$  arising from a symmetric convex coercive and differentiable penalty  $\rho$  via  $p(x) = \exp(-\rho(x))$ , and take any point  $t_0$  with  $\rho'(t_0) = \alpha_0 > 0$ . Then for all  $t_2 > t_1 \geq t_0$ , the conditional tail distribution induced by*

$p(x)$  satisfies

$$\Pr(|y| > t_2 \mid |y| > t_1) \leq \exp(-\alpha_0[t_2 - t_1]) . \quad (2.2)$$

When  $t_1$  is large, the condition  $|y| > t_1$  indicates that we are looking at an outlier. However, as shown by the theorem, *any* log-concave statistical model treats the outlier conservatively, dismissing the chance that  $|y|$  could be significantly bigger than  $t_1$ . Contrast this behavior with that of the Student's t-distribution. When  $\nu = 1$ , the Student's t-distribution is simply the Cauchy distribution, with a density proportional to  $1/(1 + y^2)$ . Then we have that

$$\lim_{t \rightarrow \infty} \Pr(|y| > 2t \mid |y| > t) = \lim_{t \rightarrow \infty} \frac{\frac{\pi}{2} - \arctan(2t)}{\frac{\pi}{2} - \arctan(t)} = \frac{1}{2}.$$

Heavy tailed distributions thus provide a fundamental advantage in cases where outliers may be particularly large, or, in the second application we discuss, very sudden trend changes may be present.

We now turn to the Kalman smoothing framework. We use the following general model for the underlying dynamics: for  $k = 1, \dots, N$

$$\begin{aligned} x_k &= g_k(x_{k-1}) + w_k \\ z_k &= h_k(z_k) + v_k \end{aligned} \quad (2.3)$$

with initial condition  $g_1(x_0) = g_0 + w_1$ , with  $g_0$  a known constant, and where  $g_k : \mathbb{R}^n \rightarrow \mathbb{R}^n$  are known smooth process functions, and  $h_k : \mathbb{R}^n \rightarrow \mathbb{R}^m$  are known smooth measurement functions. Moreover,  $w_k$  and  $v_k$  are mutually independent, and with known covariance matrices  $Q_k \in \mathbb{R}^{n \times n}$  and  $R_k \in \mathbb{R}^{m \times m}$ , respectively. Note that here we assume all the measurement vectors have consistent dimension  $m$ . There is no loss of generality compared to the standard model where the dimensions depend on  $k$ , since any measurement vector can be augmented to a standard size  $m$ , and then the phantom measurements can be disabled using the modeling interface (by setting corresponding columns and rows of  $R_k^{-1}$  to 0.)

We now briefly explain how to use Student's t error modeling to design smoothers with two important characteristics. In order to obtain smoothers that are robust to heavily contaminated data, the vector  $v_k \in \mathbb{R}^{m(k)}$  can be modeled zero-mean Student's t measurement noise (2.1) of known covariance  $R_k \in \mathbb{R}^{m(k) \times m(k)}$  and degrees of freedom  $s$ . To design smoothers that can track sudden changes in the state, the process residuals  $w_k$  are modeled using Student's t noise. These features may be employed separately or in tandem, and we always assume that the vectors  $\{w_k\} \cup \{v_k\}$  are all mutually independent.

In the next section, we design a smoother that finds the MAP estimates of  $\{x_k\}$  for a general formulation, where Student's t or least squares modeling can be used for any or all process and measurement residuals. We then specialize it to recover the applications discussed above.

**3. Generalized Smoothing Framework.** Given a sequence of column vectors  $\{u_k\}$  and matrices  $\{T_k\}$  we use the notation

$$\text{vec}(\{u_k\}) = \begin{bmatrix} u_1 \\ u_2 \\ \vdots \\ u_N \end{bmatrix}, \quad \text{diag}(\{T_k\}) = \begin{bmatrix} T_1 & 0 & \cdots & 0 \\ 0 & T_2 & \ddots & \vdots \\ \vdots & \ddots & \ddots & 0 \\ 0 & \cdots & 0 & T_N \end{bmatrix}.$$

We also make the following definitions:

$$\begin{aligned} R &= \text{diag}(\{R_k\}) \\ Q &= \text{diag}(\{Q_k\}) \quad , \quad w(x) = \text{vec}(\{x_k - g_k(x_{k-1})\}) \\ x &= \text{vec}(\{x_k\}) \quad \quad v(x) = \text{vec}(\{z_k - h_k(x_k)\}). \end{aligned}$$

In the most general case, we suppose that any of the components  $w_k^i$  or  $v_k^i$  components can be modeled either using Gaussian or Student's t distributions.

For the sake of modeling clarity, assume that *subcomponents* of measurement and innovation residuals are consistently modeled across time points  $k$ ; this gives the user the ability to select which *subvectors* of process and measurement residuals to model using Student's t, but not to assign different penalties to different time points.

Denote by  $w_k^G$  and  $w_k^S$  the subvectors of the innovation residuals  $w_k$ , and denote by  $v_k^G$  and  $v_k^S$  the subvectors of the measurement residuals  $v_k$  that are to be modeled using the Gaussian and Student's t distributions, respectively. Assume that all of these subvectors are mutually independent, and denote the corresponding covariance submatrices by  $Q_k^G$ ,  $Q_k^S$ ,  $R_k^G$ , and  $R_k^S$ . Maximizing the likelihood for this model is equivalent to minimizing the associated negative log likelihood

$$-\ln \mathbf{p}(\{\nu_k^G\}, \{\nu_k^S\}, \{w_k^G\}, \{w_k^S\}),$$

which can be explicitly written as follows:

$$\sum_{k=1}^N s \ln \left[ 1 + \frac{\|v_k^S\|_{(R_k^S)^{-1}}^2}{s} \right] + \|v_k^G\|_{(R_k^G)^{-1}}^2 + r \ln \left[ 1 + \frac{\|w_k^S\|_{(Q_k^S)^{-1}}^2}{r} \right] + \|w_k^G\|_{(Q_k^G)^{-1}}^2 \quad (3.1)$$

where  $s$  and  $r$  are degree of freedom parameters corresponding to  $v_k^S$  and  $w_k^S$ .

A first-order accurate affine approximation to our model with respect to direction  $d = \text{vec}\{d_k\}$  near a fixed state sequence  $x$  is given by

$$\begin{aligned} \tilde{w}(x; d) &= \text{vec}(\{x_k - g_k(x_{k-1}) - g_k^{(1)}(x_{k-1})d_k\}), \\ \tilde{v}(x; d) &= \text{vec}(\{z_k - h_k(x_k) - h_k^{(1)}(x_k)d_k\}). \end{aligned}$$

Set  $Q_{N+1} = I_n$  and  $g_{N+1}(x_N) = 0$  (where  $I_n$  is the  $n \times n$  identity matrix) so that the formulas are also valid for  $k = N + 1$ .

We minimize the nonlinear nonconvex objective in (3.1) by iteratively solving quadratic programming (QP) subproblems of the form:

$$\min \quad \frac{1}{2} d^T C d + a^T d \quad \text{w.r.t } d \in \mathbb{R}^{nN}, \quad (3.2)$$

where  $a$  is the gradient of objective (4.1) with respect to  $x$  and  $C$  has the form

$$C = \begin{bmatrix} C_1 + H_1 & A_2^T & 0 & & \\ A_2 & C_2 + H_2 & A_3^T & & 0 \\ 0 & & \ddots & \ddots & \\ & 0 & A_N & C_N + H_N & \end{bmatrix}, \quad (3.3)$$

Note that this matrix is symmetric block tridiagonal. This structure is essential to the computational results for a wide variety of Kalman filtering and smoothing algorithms; it was noted early on in [12, 31].

In order to fully describe  $C_k$  and  $A_k$ , first let  $\mathcal{W}^G$ ,  $\mathcal{W}^S$  denote the indices associated to all subvectors  $w_k^G$  and  $w_k^S$  within  $w_k$ . For example, if the Student's  $t$  density is used for all measurement residuals, and the Gaussian penalty is used for all process residuals, then  $\mathcal{W}^G = \{1, \dots, n\}$ ,  $\mathcal{W}^S = \emptyset$ .

Now define with  $A_k, C_k, H_k \in \mathbb{R}^{n \times n}$  as follows:

$$\begin{aligned} A_k(\mathcal{W}^S, \mathcal{W}^S) &= -\frac{r(Q_k^S)^{-1}(g_k^{(1)})^S}{r + \|w_k^S\|_{(Q_k^S)^{-1}}^2} \\ A_k(\mathcal{W}^G, \mathcal{W}^G) &= -(Q_k^G)^{-1}(g_k^{(1)})^G \end{aligned} \quad (3.4)$$

$$\begin{aligned} C_k(\mathcal{W}^G, \mathcal{W}^G) &= ((g_{k+1}^{(1)})^G)^T (Q_{k+1}^G)^{-1} (g_{k+1}^{(1)})^G + (Q_k^G)^{-1} \\ C_k(\mathcal{W}^S, \mathcal{W}^S) &= \frac{r((g_{k+1}^{(1)})^S)^T (Q_{k+1}^S)^{-1} (g_{k+1}^{(1)})^S}{r + \|w_{k+1}^S\|_{(Q_{k+1}^S)^{-1}}^2} + \frac{r(Q_k^S)^{-1}}{r + \|w_k^S\|_{(Q_k^S)^{-1}}^2} \\ H_k &= \frac{s((h_k^{(1)})^S)^T (R_k^S)^{-1} (h_k^{(1)})^S}{(s + \|v_k^S\|_{(R_k^S)^{-1}}^2)} + ((h_k^{(1)})^G)^T (R_k^G)^{-1} (h_k^{(1)})^G. \end{aligned} \quad (3.5)$$

The entries of  $A_k$  and  $C_k$  not explicitly defined in (3.4) and (3.5) are set to 0.

The Hessian approximation terms  $H_k$  in (3.6) are motivated in Section 5, and are crucial to both practical performance and theoretical convergence analysis. The solutions to the subproblem (3.2) have the form  $d = -C^{-1}a$ , and can be found in an efficient and numerically stable manner in  $O(n^3N)$  steps, since  $C$  is tridiagonal and positive definite (see [8]).

**4. Special cases.** We now show how the general framework of the previous section can be specialized to obtain three smoothers. The first two are T-Robust and T-Trend, which are presented in [5]. The third is a new smoother where *all* residuals and innovations are modeled using Student's  $t$ .

The objective corresponding to T-Robust is obtained from (3.1) by taking  $w_k^G = w_k$ ,  $w_k^S = 0$ ,  $v_k^G = 0$ ,  $v_k^S = v_k$ :

$$\frac{1}{2} \sum_{k=1}^N s \ln \left[ 1 + \frac{\|v_k\|_{R_k^{-1}}^2}{s} \right] + \|w_k\|_{Q_k^{-1}}^2. \quad (4.1)$$

The terms  $A_k, C_k, H_k$  in (3.4)–(3.6) become

$$\begin{aligned} A_k &= -Q_k^{-1} g_k^{(1)}, \\ C_k &= Q_k^{-1} + (g_{k+1}^{(1)})^T Q_{k+1}^{-1} g_{k+1}^{(1)}, \\ H_k &= \frac{s(h_k^{(1)})^T R_k^{-1} h_k^{(1)}}{(s + \|v_k\|_{R_k^{-1}}^2)}. \end{aligned} \quad (4.2)$$

The objective corresponding to T-Trend is obtained from (3.1) by taking  $w_k^G = 0$ ,  $w_k^S = w_k$ ,  $v_k^G = v_k$ ,  $v_k^S = 0$ :

$$\frac{1}{2} \sum_{k=1}^N r \ln \left[ 1 + \frac{\|w_k\|_{Q_k^{-1}}^2}{r} \right] + \|v_k\|_{R_k^{-1}}^2. \quad (4.3)$$

The terms  $A_k, C_k, H_k$  in (3.4)—(3.6) become

$$\begin{aligned} A_k &= -\frac{rQ_k^{-1}g_k^{(1)}}{r + \|w_k\|_{Q_k^{-1}}^2}, \\ C_k &= \frac{rQ_k^{-1}}{r + \|w_k\|_{Q_k^{-1}}^2} + \frac{r(g_{k+1}^{(1)})^T Q_{k+1}^{-1} g_{k+1}^{(1)}}{r + \|w_{k+1}\|_{Q_{k+1}^{-1}}^2}, \\ H_k &= (h_k^{(1)})^T R_k^{-1} h_k^{(1)}. \end{aligned} \quad (4.4)$$

Finally, we can apply Student's t to all process and measurement residuals by taking  $w_k^G = 0$ ,  $w_k^S = w_k$ ,  $v_k^G = 0$ ,  $v_k^S = v_k$  to obtain

$$\frac{1}{2} \sum_{k=1}^N r_k \ln \left[ 1 + \frac{\|w_k\|_{Q_k^{-1}}^2}{r_k} \right] + s_k \ln \left[ 1 + \frac{\|v_k\|_{R_k^{-1}}^2}{s_k} \right] \quad (4.5)$$

The terms  $A_k, C_k, H_k$  in (3.4)—(3.6) become

$$\begin{aligned} A_k &= -\frac{rQ_k^{-1}g_k^{(1)}}{r + \|w_k\|_{Q_k^{-1}}^2}, \\ C_k &= \frac{rQ_k^{-1}}{r + \|w_k\|_{Q_k^{-1}}^2} + \frac{r(g_{k+1}^{(1)})^T Q_{k+1}^{-1} g_{k+1}^{(1)}}{r + \|w_{k+1}\|_{Q_{k+1}^{-1}}^2}, \\ H_k &= \frac{s(h_k^{(1)})^T R_k^{-1} h_k^{(1)}}{(s + \|v_k\|_{R_k^{-1}}^2)}. \end{aligned} \quad (4.6)$$

**5. Algorithm and Global Convergence.** When models  $g_k$  and  $h_k$  are linear, we can compare the algorithmic scheme proposed in the previous sections with the method in [13]. The latter uses the random information matrix (random Hessian) in place of the matrix  $C$  defined above, and recommends using the expected (Fisher) information when the full Hessian is indefinite. When the densities for  $w_k$  and  $v_k$  are Gaussian, this is equivalent to using Newton's method when possible, and using Gauss-Newton when the Hessian is indefinite. In general, using the expected information is known as the method of Fisher's scoring. In the Student's t-case, the scalar Fisher information matrix is computed in [19] to be

$$\frac{s+1}{s+3} \sigma^{-2}, \quad (5.1)$$

where  $\sigma^2$  is the variance and  $s$  is the degrees of freedom. The authors of [13] proposed using (5.1) as the Hessian approximation when the full Hessian is indefinite. Implementing this approach would effectively replace the terms  $\|w_k\|_2^2$  or  $\|v_k\|_2^2$ , present in the denominators of  $H_k$  and  $A_k$  (see 4.2 and 4.4), with terms that depend only on  $s_k$  and  $r_k$ , the degrees of freedom. So while the random information (Hessian) matrix can become indefinite, the Fisher information is insensitive to outliers, and fails to down-weight their contributions to the Hessian approximation.

To overcome these drawbacks, and find a middle ground between using the full Hessian and using a very rough approximation, we propose a Gauss-Newton method that is able to incorporate the relative size information of the residuals into the Hessian

approximation. In the rest of this section we provide the details for the application of this method and a proof of convergence.

As in [2], the convergence theory is based upon the versatile convex-composite techniques developed in [9]. We begin by choosing the convex-composite structure for objective (3.1). We write it in the convex-composite form  $K = \rho \circ F$ , with smooth  $F$  and convex  $\rho$ :

$$\rho \begin{pmatrix} c \\ u \end{pmatrix} = c + \frac{1}{2} \|u\|_{B^{-1}}^2 + \delta_{\mathbb{R}_+}(c) \quad (5.2)$$

$$F(x) = \begin{pmatrix} f(x) \\ w^G(x) \\ v^G(x) \end{pmatrix} \quad (5.3)$$

$$f(x) = \frac{1}{2} \sum_{k=1}^N s \ln \left[ 1 + \frac{\|v_k^S\|_{(R_k^S)^{-1}}^2}{s} \right] + \sum_{k=1}^N r \ln \left[ 1 + \frac{\|w_k^S\|_{(Q_k^S)^{-1}}^2}{r} \right]. \quad (5.4)$$

Note that the range of  $f$  is  $\mathbf{R}_+$ , and  $\rho$  is coercive on its domain. The terms indexed with superscript  $S$  in (3.5) and (3.6) combine to form a positive definite approximation to the Hessian of  $f$ . To see this, consider the scalar function

$$\kappa(x) := \frac{1}{2} \ln(1 + x^2/r).$$

The second derivative of this function in  $x$  is given by

$$\frac{(r + x^2) - 2x^2}{(r + x^2)^2} = \frac{r - x^2}{(r + x^2)^2} \quad (5.5)$$

and is only positive on  $(-\sqrt{r}, \sqrt{r})$ . There are two reasonable globally positive approximations to take. The first,

$$\frac{r}{(r + x^2)^2},$$

simply ignores the subtracted term  $-x^2$ . In practice, we found this approximation to be too aggressive. Instead, we drop the  $2x^2$  from the left of (5.5) to obtain the approximation

$$\frac{(r + x^2)}{(r + x^2)^2} = \frac{1}{(r + x^2)}. \quad (5.6)$$

Similarly, the terms indexed by superscript  $S$  in (3.5) and (3.6) provide globally positive definite approximations to the Hessian of  $f$ , using the strategy in (5.6). This strategy offers a significant computational advantage—the Hessian approximation that is built up down-weights the contributions of outliers, helping the algorithm proceed faster to the solution. As we shall see, these terms are also essential for the general convergence theory.

Our approach exploits the objective structure by iteratively linearizing  $F$  about the iterates  $x^k$  and solving the *direction finding subproblem*

$$\min_{d \in \mathbb{R}^{n_N}} \rho(F(x^k) + F^{(1)}(x^k)d) + \frac{1}{2} d^T U(x^k) d, \quad (5.7)$$



where  $U(x^k)$  is a symmetric positive semidefinite matrix that depends continuously on  $x^k$ . For any smoother in the framework of section 3, problem (5.7) can be solved with a single block-tridiagonal solve of the system (3.2), yielding descent directions  $d$  for the objective  $K(x)$ .

We now develop a general convergence theory for convex-composite methods to establish the overall convergence to a stationary point of  $K(x)$ . This theory is in the spirit of [2] and [9], and allows the inclusion of the quadratic term  $\frac{1}{2}d^T U(x^k)d$  in (5.7). This term was not necessary in [2], but is crucial here. Note that the theory does not rely at all on the technique used to solve the direction finding subproblem, and so the theory in this paper applies to the algorithm in [2] by taking  $U = 0$ .

Recall from [9] that the first-order necessary condition for optimality in the convex composite problem involving  $K(x)$  is

$$0 \in \partial K(x) = \partial \rho(F(x)) F^{(1)}(x)$$

where  $\partial K(x)$  is the generalized subdifferential of  $K$  at  $x$  [23] and  $\partial \rho(F(x))$  is the convex subdifferential of  $\rho$  at  $F(x)$  [22]. Elementary convex analysis gives us the equivalence

$$0 \in \partial K(x) \quad \Leftrightarrow \quad K(x) = \inf_d \rho \left( F(x) + F^{(1)}(x)d \right) .$$

For the general smoothing class of interest, it is desirable to modify this objective by including curvature information, yielding the problem (5.7). We define the difference function

$$\Delta(x; d) = \rho \left( F(x) + F^{(1)}(x)d \right) + \frac{1}{2}d^T U(x)d - K(x) , \quad (5.8)$$

where  $U(x)$  is positive semidefinite and varies continuously with  $x$ . Note that  $\Delta(x; d)$  is a convex function of  $d$  that is bounded below, hence the optimal value

$$\Delta^*(x) = \inf_d \Delta(x; d) \quad (5.9)$$

is well defined regardless of the existence of a solution. If  $\Delta^*(x) = 0$ , then  $0 \in \arg \min_d \Delta(x; d)$ . Hence, by [9, Theorem 3.6],  $\Delta^*(x) = 0$  if and only if  $0 \in \partial K(x)$ .

Given  $\eta \in (0, 1)$ , we define a set of search directions at  $x$  by

$$D(x, \eta) = \{ d \mid \Delta(x; d) \leq \eta \Delta^*(x) \} . \quad (5.10)$$

Note that if there is a  $d \in D(x, \eta)$  such that  $\Delta(x; d) \geq -\eta\varepsilon$ , then  $\Delta^*(x) \geq -\varepsilon$ . These ideas motivate the following algorithm.

ALGORITHM 5.1. *Gauss-Newton Algorithm.*

*The inputs to this algorithm are*

- $x^0 \in \mathbb{R}^{N_n}$ : initial estimate of state sequence
- $\varepsilon \geq 0$ : overall termination criterion
- $\eta \in (0, 1)$ : search direction selection parameter
- $\beta \in (0, 1)$ : step size selection parameter
- $\gamma \in (0, 1)$ : line search step size factor

*The steps are as follows:*

1. Set the iteration counter  $\nu = 0$ .

2. (Gauss-Newton Step) Find  $d^\nu$  in the set  $D(x^\nu, \eta)$  in 5.10. Set  $\Delta_\nu = \Delta(x^\nu; d^\nu)$  in 5.8 and Terminate if  $\Delta_\nu \geq -\varepsilon$ .
3. (Line Search) Set

$$\begin{aligned} t_\nu &= \max \gamma^i \\ \text{s.t. } i &\in \{0, 1, 2, \dots\} \text{ and} \\ \text{s.t. } \rho(F(x^\nu + \gamma^i d^\nu)) &\leq \rho(F(x^\nu)) + \beta \gamma^i \Delta_\nu. \end{aligned}$$

4. (Iterate) Set  $x^{\nu+1} = x^\nu + t_\nu d^\nu$  and return to Step 2.

We now present a general global convergence theorem that covers any smoother in section 3. This theorem also generalizes [2, Theorem 5.1] to include positive semidefinite curvature terms in the Gauss-Newton framework.

THEOREM 5.1. *Define*

$$\Lambda := \{u | \rho(u) \leq K(x^0)\} \quad (5.11)$$

and suppose that there exists a  $\tau > 0$  such that  $F^{(1)}$  is bounded and uniformly continuous on the set

$$S_0 := \overline{co} \left( F^{-1}(\Lambda) \right) + \tau \mathbb{B}. \quad (5.12)$$

If  $\{x^\nu\}$  is a sequence generated by the Gauss-Newton Algorithm 5.1 with initial point  $x^0$  and  $\varepsilon = 0$ , then one of the following must occur:

- (i) The algorithm terminates finitely at a point  $x^\nu$  with  $0 \in \partial K(x^\nu)$ .
- (ii) The sequence  $\|d^\nu\|$  diverges to  $+\infty$ .
- (iii)  $\lim_{\nu \in I} \Delta_\nu = \lim_{\nu \in I} \Delta^*(x^\nu) = 0$  for every subsequence  $I$  for which the set  $\{d^\nu | \nu \in I\}$  is bounded.

Moreover, if  $\bar{x}$  is any cluster point of a subsequence  $I \subset \mathbf{Z}_+$  such that the subsequence  $\{d^\nu | \nu \in I\}$  is bounded, then  $0 \in \partial K(\bar{x})$ .

*Proof.* We will assume that none of (i), (ii), (iii) occur and establish a contradiction. Then there is a subsequence  $I$  such that

$$\sup_{\nu \in I} \|d_\nu\| < \infty \quad \text{and} \quad \sup_{\nu \in I} \Delta_\nu \leq \zeta < 0.$$

Since  $K(x^\nu)$  is a decreasing sequence that is bounded below by 0, we know that the differences  $K(x^{\nu+1}) - K(x^\nu) \rightarrow 0$ . Therefore, by Step 3) of Algorithm 5.1,  $\zeta t_\nu \Delta_\nu \rightarrow 0$ , which implies that  $t_{\nu \in I} \rightarrow 0$ . Without loss of generality we may assume that  $t_\nu \leq 1$  and  $t_\nu \|d_\nu\| \leq \gamma\tau$  for all  $\nu \in I$ . Hence for all  $\nu \in I$ ,

$$\begin{aligned} \|F(x^\nu + t_\nu \gamma^{-1} d^\nu) - F(x^\nu)\| &\leq t_\nu \gamma^{-1} \int_0^1 \|F'(x^\nu + st_\nu \gamma^{-1} d^\nu)\| \|d^\nu\| ds \\ &\leq \tau M, \end{aligned}$$

where  $M$  is a bound on  $F'$  over  $S_0$ . Let  $K$  be a Lipschitz constant for  $\rho$  over the compact set  $\Lambda + \tau M \mathbb{B}$ . Again by Step 3) of Algorithm 5.1, for all  $\nu \in I$ ,

$$\begin{aligned} \beta \gamma^{-1} t_\nu \Delta_\nu &\leq \rho(F(x^\nu + t_\nu \gamma^{-1} d^\nu)) - \rho(F(x^\nu)) \\ &\leq t_\nu \gamma^{-1} \Delta_\nu + K \|F(x^\nu + t_\nu \gamma^{-1} d^\nu) - F(x^\nu) - t_\nu \gamma^{-1} F^{(1)}(x^\nu) d^\nu\| \\ &= t_\nu \gamma^{-1} \Delta_\nu + t_\nu \gamma^{-1} K \left\| \int_0^1 \left( F^{(1)}(x^\nu + st_\nu \gamma^{-1} d^\nu) - F^{(1)}(x^\nu) \right) d^\nu ds \right\| \\ &\leq t_\nu \gamma^{-1} \left( \Delta_\nu + K \omega(t_\nu \gamma^{-1} \|d_\nu\|) \|d_\nu\| \right), \end{aligned}$$

where  $\omega$  is the modulus of continuity of  $F'$  on  $S_0$ . Rearranging, we obtain

$$0 \leq (1 - \beta)\Delta_\nu + K\omega(t_\nu\gamma^{-1}\|d_\nu\|)\|d_\nu\|.$$

Taking the limit for  $\nu \in I$ , we obtain the contradiction  $0 \leq (1 - \beta)\zeta$ . Hence,  $\lim_{\nu \in I} \Delta_\nu = 0$ , which implies that  $\lim_{\nu \in I} \Delta^*(x^\nu) = 0$ , since  $\Delta_\nu \leq \eta\Delta^*(x^\nu) \leq 0$ .

Finally, suppose that  $\bar{x}$  is a cluster point of a sequence  $I \subset \mathbf{Z}_+$  for which  $\{d^\nu\}$  is bounded. Without loss of generality, there exists a  $\bar{d}$  such that  $(x^\nu, d^\nu)_{\nu \in I} \rightarrow (\bar{x}, \bar{d})$ . For all  $d \in \mathbb{R}^{Nn}$ ,

$$\begin{aligned} \Delta_\nu &= \rho\left(F(x^\nu) + F^{(1)}(x^\nu)d^\nu\right) + \frac{1}{2}\|d^\nu\|_{U^\nu}^2 - \rho(F(x^\nu)) \\ &\leq \eta\Delta^*(x^\nu) \\ &\leq \eta\left(\rho\left(F(x^\nu) + F^{(1)}(x^\nu)d\right) + \frac{1}{2}\|d\|_{U^\nu}^2 - \rho(F(x^\nu))\right), \end{aligned}$$

where  $U^\nu = U(x^\nu)$ . Taking the limit over  $J$  gives

$$\begin{aligned} 0 &= \rho\left(F(\bar{x}) + F^{(1)}(\bar{x})\bar{d}\right) + \frac{1}{2}\|\bar{d}\|_{\bar{U}}^2 - \rho(F(\bar{x})) \\ &\leq \eta\left(\rho\left(F(\bar{x}) + F^{(1)}(\bar{x})d\right) + \frac{1}{2}\|d\|_{\bar{U}}^2 - \rho(F(\bar{x}))\right), \end{aligned}$$

where  $\bar{U} = U(\bar{x})$ . Since  $d$  was chosen arbitrarily, it must be the case that  $\Delta^*(\bar{x}) = 0$ , which implies that  $0 \in \partial K$  by [9, Theorem 3.6].  $\square$

A stronger convergence result is possible under stronger assumptions on  $F$  and  $F^{(1)}$ .

**COROLLARY 5.2.** *Suppose that  $F^{-1}(\Lambda) = \{x \mid F(x) \in \Lambda\}$  is bounded, and there exists  $0 < \lambda_{\min}$  such that*

$$\forall x \in F^{-1}(\Lambda), \quad 0 < \lambda_{\min}\|d\|^2 \leq d^T U(x)d \quad \forall d \in \text{Null}(F^{(1)}(x)). \quad (5.13)$$

*If  $\{x^\nu\}$  is a sequence generated by Algorithm 5.1 with initial point  $x^0$  and  $\varepsilon = 0$ , then  $\{x^\nu\}$  and  $\{d^\nu\}$  are bounded and either the algorithm terminates finitely at a point  $x^\nu$  with  $0 \in \partial K(x^\nu)$ , or  $\Delta_\nu \rightarrow 0$  as  $\nu \rightarrow \infty$ , and every cluster point  $\bar{x}$  of the sequence  $\{x^\nu\}$  satisfies  $0 \in \partial K(\bar{x})$ .*

*Proof.* First note that  $F^{-1}(\Lambda)$  is closed since  $F$  is continuous, and therefore  $F^{-1}(\Lambda)$  is compact, since by assumption it is bounded. Hence  $S_0$  (see (5.12)) is also compact. Therefore,  $F^{(1)}$  is uniformly continuous and bounded on  $S_0$  which implies that the hypotheses of Theorem 5.1 are satisfied, and so one of (i)-(iii) must hold. If (i) holds we are done, so we will assume that the sequence  $\{x^\nu\}$  is infinite. Since  $\{x^\nu\} \subset F^{-1}(\Lambda)$ , this sequence is bounded. We now show that the sequence  $\{d^\nu\}$  of search directions is also bounded.

Suppose that (5.13) holds. For any direction  $d^\nu$ , note that  $d^\nu$  satisfies

$$\rho\left(F(x^\nu) + F^{(1)}(x^\nu)d^\nu\right) + \frac{1}{2}\|d^\nu\|_{U^\nu}^2 \leq \rho(F(x^\nu)) \leq \rho(F(x^0)). \quad (5.14)$$

Since  $\rho \geq 0$ , we have

$$\{F(x^\nu)\} \subset \Lambda \quad \text{and} \quad \{F(x^\nu) + F^{(1)}(x^\nu)d^\nu\} \subset \Lambda \quad (5.15)$$

and

$$\left\{\frac{1}{2}(d^\nu)^T U^\nu d^\nu\right\} \leq \rho(F(x^0)) \quad \forall \nu. \quad (5.16)$$

Suppose that the  $\{d^\nu\}$  is unbounded. Then without loss of generality, there exists a subsequence  $I$ , a unit vector  $u$ , and a vector  $\bar{x} \in F^{-1}(\Lambda)$  such that  $\lim_{\nu \in I} d^\nu / \|d^\nu\| \rightarrow u$  and  $\lim_{\nu \in I} x^\nu \rightarrow \bar{x}$ . Since  $\Lambda$  is bounded, (5.15) implies that  $F^{(1)}(\bar{x})u = 0$ , so  $u \in \text{Nul}(F^{(1)}(\bar{x}))$ , and therefore

$$0 < \lambda_{\min} \leq u^T U(\bar{x})u.$$

On the other hand, by (5.16),  $\frac{1}{2} \left( \frac{d^\nu}{\|d^\nu\|} \right)^T U^\nu \left( \frac{d^\nu}{\|d^\nu\|} \right) \leq \frac{\rho(F(x^0))}{\|d^\nu\|^2}$  and so in the limit we have the contradiction

$$0 < \lambda_{\min} \leq u^T U(\bar{x})u \leq 0.$$

Hence  $d^\nu$  are bounded. The result now follows from Theorem 5.1.

□

We now show that all smoothers of section 3 satisfy the required assumptions of Theorem 5.1 and Corollary (5.2).

**COROLLARY 5.3** (Smoother Satisfaction). *Suppose that the process and measurement functions  $g_k$  and  $h_k$  in (2.3) are twice continuously differentiable. Then for  $F$  given in (5.3),  $F^{(1)}$  is bounded and uniformly continuous on  $S_0$  in (5.12). Moreover, the hypotheses of Corollary 5.2 hold if for all  $x$  in  $F^{-1}(\Lambda)$  and for all  $k$ , there exists  $\eta$  such that*

$$0 < \eta < \sigma_{\min}(G^S(x)), \quad G^S(x) := \begin{bmatrix} I & 0 & 0 & 0 \\ -(g_k^{(1)}(x))^S & I & 0 & 0 \\ 0 & \ddots & \ddots & \ddots \\ 0 & 0 & -(g_k^{(N-1)}(x))^S & I \end{bmatrix}$$

*Proof.* We first show that both  $\Lambda$  and  $F^{-1}(\Lambda)$  are bounded. The first claim follows immediately by the coercivity of  $\rho$  in (5.2). To verify the second claim, we will show that for any sequence of  $x^\nu$  with  $\|x^\nu\| \rightarrow \infty$ , we can find a subsequence  $J$  such that  $\lim_{\nu \in J} \|w^\nu\| = \infty$ , which implies the existence of subsequence  $I$  such that either  $\lim_{\nu \in I} \|w^G\| = \infty$  or  $\lim_{\nu \in I} f(x^\nu) = \infty$ . In particular there does not exist an unbounded sequence  $\{x^\nu\}$  with  $F(x^\nu) \subset \Lambda$ , and therefore  $F^{-1}(\Lambda)$  must be bounded.

If  $\|x^\nu\| \rightarrow \infty$ , we can find an index  $k \in [1, \dots, N]$  and subsequence  $J$  such that  $\lim_{\nu \in J} \|x_k^\nu\| = \infty$ . Now, either  $\lim_{\nu \in J} \|w_k^\nu\| = \infty$  and we are done, or  $\lim_{\nu \in J} \|g_k(x_{k-1}^\nu)\| = \infty$ , so  $\lim_{\nu \in J} \|x_{k-1}^\nu\| = \infty$ . Iterating this argument, we arrive at the limiting case  $w_1^\nu = x_1^\nu - x_1^0$ , and so if all  $\|w_j^\nu\|$  are bounded for  $j > 1$ , we can guarantee that  $\lim_{\nu \in J} \|w_1^\nu\| = \infty$ .

Since  $F$  is twice continuously differentiable by the hypotheses on  $g$  and  $h$ , the boundedness of  $F^{-1}(\Lambda)$  establishes the boundedness and uniform continuity of  $F^{(1)}$  on  $S_0$  in (5.12) for any  $\tau > 0$ .

It remains to show that condition (5.13) is satisfied. Let  $\mathcal{W}^G, \mathcal{W}^S$  denote the indices associated to all subvectors  $w_k^G$  and  $w_k^S$  within  $w_k$ . If  $d \in \text{Null}(F^{(1)}(x))$ , then necessarily  $d_{\mathcal{W}^G} = 0$ . This is simply because  $F^{(1)}$  is nonsingular on  $\mathcal{W}^G$ , since it contains the sub matrix

$$G^G(x) := \begin{bmatrix} I & 0 & & \\ -(g_2^{(1)})^G(x_1) & I & \ddots & \\ & \ddots & \ddots & 0 \\ & & -(g_N^{(1)})^G(x_{N-1}) & I \end{bmatrix},$$

which is the standard process matrix  $G$  projected to those coordinates where Gaussian modeling is applied. To finish the analysis, we present the full form of the matrix  $U$  restricted to  $\mathcal{W}^S$ :

$$U = \begin{bmatrix} U_1 & A_2^T & 0 & \\ A_2 & U_2 & A_3^T & 0 \\ 0 & \ddots & \ddots & \ddots \\ & 0 & A_N & U_N \end{bmatrix} + \text{diag}(\{H_k\}), \quad (5.17)$$

where

$$\begin{aligned} A_k &= -\frac{r(Q_k^S)^{-1}(g_k^{(1)})^S}{r + \|w_k^S\|_{(Q_k^S)^{-1}}^2} \\ U_k &= \frac{r((g_{k+1}^{(1)})^S)^T (Q_{k+1}^S)^{-1} (g_{k+1}^{(1)})^S}{r + \|w_{k+1}^S\|_{(Q_{k+1}^S)^{-1}}^2} + \frac{r(Q_k^S)^{-1}}{r + \|w_k^S\|_{(Q_k^S)^{-1}}^2} \\ H_k &= \frac{s((h_k^{(1)})^S)^T (R_k^S)^{-1} (h_k^{(1)})^S}{(s + \|v_k^S\|_{(R_k^S)^{-1}}^2)} \end{aligned} \quad (5.18)$$

Note that we can write the first summand in (5.17) as  $(G^S)^T \tilde{Q}^{-1} G^S$ , where

$$\tilde{Q}^{-1} := \text{diag}(\{\tilde{Q}_k^{-1}\}), \quad \tilde{Q}_k^{-1} = \frac{r(Q_k^S)^{-1}}{r + \|w_k^S\|_{(Q_k^S)^{-1}}^2}.$$

Since  $F^{-1}(\Lambda)$  is bounded, the denominators of  $\tilde{Q}_k^{-1}$  are bounded, and so eigenvalues of  $\tilde{Q}_k^{-1}$  are bounded from below, and the singular values of  $G^S$  are bounded from above.

We now have

$$0 < \eta_{\min} \leq \sigma_{\min}(G^S) \leq \sigma_{\max}(G^S) \leq \eta_{\max}$$

for all  $x$ , where the upper bound follows from Theorem [4, 2.2] together with compactness of  $F^{-1}(\Lambda)$ .

Then, by [4, Theorem 2.1], we have

$$\kappa((G^S)^T \tilde{Q}^{-1} G^S) \leq \frac{\lambda_{\max}(\tilde{Q}^{-1}) \eta_{\max}^2}{\lambda_{\min}(\tilde{Q}^{-1}) \eta_{\min}^2}.$$

for all  $x \in F^{-1}(\Lambda)$ . This completes the proof.  $\square$

**REMARK 5.2.** *One can also consider conditions on the individual  $g_k^S$  that can produce a lower bound  $\eta$  on  $G^S$ , as required by Corollary 5.3. One such condition is*

$$0 < \eta \leq \left\{ 1 + \sigma_{\min}^2(g_{k+1}^{(1)}) - \sigma_{\max}(g_k^{(1)}) - \sigma_{\max}(g_{k+1}^{(1)}) \right\} \quad (5.19)$$

*If this condition is satisfied, then by Theorem [4, 2.2],  $\eta < \sigma_{\min}(G^S)$ . However, this condition is sufficient, and may not be necessary.*

## 6. Numerical Experiments.

**6.1. T-Robust Smoother: function reconstruction using splines.** In this section we compare the new T-robust smoother with the  $\ell_2$ -Kalman smoother [8] and with the  $\ell_1$ -Laplace robust smoother [2], both implemented in [1]. The *ground truth* for this simulated example is

$$x(t) = [-\cos(t) \quad -\sin(t)]^T.$$

The time between measurements is a constant  $\Delta t$ . We model the two components of the state as the first and second integrals of white noise, so that

$$g_k(x_{k-1}) = \begin{bmatrix} 1 & 0 \\ \Delta t & 1 \end{bmatrix} x_{k-1}, \quad Q_k = \begin{bmatrix} \Delta t & \Delta t^2/2 \\ \Delta t^2/2 & \Delta t^3/3 \end{bmatrix}.$$

This stochastic model for function reconstruction underlies the Bayesian interpretation of cubic smoothing splines, see [28] for details.

The measurement model for the conditional mean of measurement  $z_k$  given state  $x_k$  is defined by

$$h_k(x_k) = [0 \quad 1] x_k = x_{2,k}, \quad R_k = \sigma^2,$$

where  $x_{2,k}$  denotes the second component of  $x_k$ ,  $\sigma^2 = 0.25$  for all experiments, and the degrees of freedom parameter  $k$  was set to 4 for the Student's t methods.

The measurements  $\{z_k\}$  were generated as a sample from

$$z_k = x_2(t_k) + v_k, \quad t_k = 0.04\pi \times k$$

where  $k = 1, 2, \dots, 100$ . The measurement noise  $v_k$  was generated according to the following schemes.

1. **Nominal:**  $v_k \sim \mathbf{N}(0, 0.25)$ .

2. **Gaussian contamination**

$$v_k \sim (1 - p)\mathbf{N}(0, 0.25) + p\mathbf{N}(0, \phi),$$

for  $p \in \{0.1, 0.2, 0.5\}$  and  $\phi \in \{1, 4, 10, 100\}$ .

3. **Uniform contamination**

$$v_k \sim (1 - p)\mathbf{N}(0, 0.25) + p\mathbf{U}(-10, 10),$$

for  $p \in \{0.1, 0.2, 0.5\}$ .

Each experiment was performed 1000 times. Table 6.1 presents the results for our simulated fitting showing the median Mean Squared Error (MSE) value and a quantile interval containing 95% of the results. The MSE is defined by

$$\frac{1}{N} \sum_{k=1}^N [x_1(t_k) - \hat{x}_{1,k}]^2 + [x_2(t_k) - \hat{x}_{2,k}]^2, \quad (6.1)$$

where  $\{\hat{x}_k\}$  is the corresponding estimating sequence.

From Table 6.1 one can see that T-Robust and the  $\ell_1$ -smoother perform as well as the (optimal)  $\ell_2$ -smoother at nominal conditions, and that both continue to perform at that same level for a variety of outlier generating scenarios. T-Robust always

TABLE 6.1

Function reconstruction via spline: median MSE over 1000 runs and intervals containing 95% of MSE results.

Outlier	p	$\ell_2$ MSE	$\ell_1$ MSE	Student's t MSE
Nominal	—	.04(.02, .1)	.04(.01, .1)	.04(.01, .09)
$\mathbf{N}(0, 1)$	.1	.06(.02, .12)	.04(.02, .10)	.04(.02, .10)
$\mathbf{N}(0, 4)$	.1	.09(.04, .29)	.05(.02, .12)	.04(.02, .11)
$\mathbf{N}(0, 10)$	.1	.17(.05, .55)	.05(.02, .13)	.04(.02, .11)
$\mathbf{N}(0, 100)$	.1	1.3(.30, 5.0)	.05(.02, .14)	.04(.02, .11)
$\mathbf{U}(-10, 10)$	.1	.47(.12, 1.5)	.05(.02, .13)	.04(.02, .10)
$\mathbf{N}(0, 10)$	.2	.32(.11, .95)	.06(.02, .19)	.05(.02, .16)
$\mathbf{N}(0, 100)$	.2	2.9(.94, 8.5)	.07(.02, .22)	.05(.02, .14)
$\mathbf{U}(-10, 10)$	.2	1.1(.36, 3.0)	.07(.03, .26)	.05(.02, .13)
$\mathbf{N}(0, 10)$	.5	.74(.29, 1.9)	.13(.05, .49)	.10(.04, .45)
$\mathbf{N}(0, 100)$	.5	7.7(2.9, 18)	.21(.06, 1.6)	.09(.03, .44)
$\mathbf{U}(-10, 10)$	.5	2.6(1.0, 5.8)	.20(.06, 1.4)	.10(.03, .44)

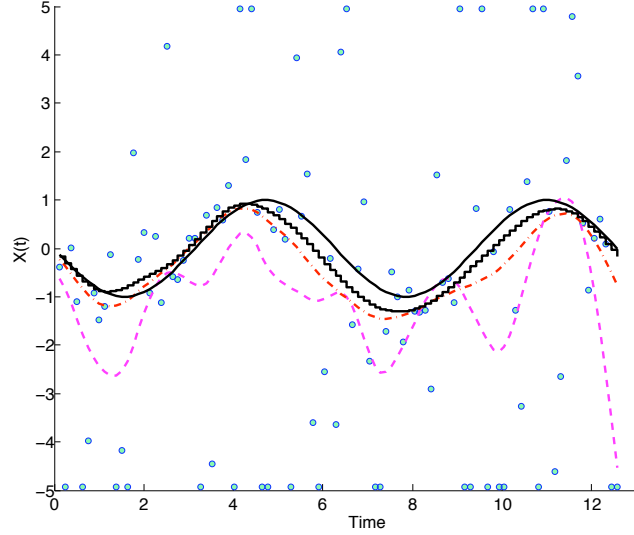


FIG. 6.1. Function reconstruction via spline: performance of  $\ell_2$  Kalman smoother (dash),  $\ell_1$ -Laplace Robust smoother (dash-dot), and T-Robust (stair-case solid) on contaminated normal model with 50% outliers distributed uniformly on  $[-10, 10]$ . True state  $x(t)$  is drawn as solid line. Measurements appear as 'o' symbols, and all measurements visible off of the true state are outliers in this case. Values outside  $[-5, 5]$  are plotted on the axis limits.

performs at least as well as the  $\ell_1$ -smoother, and it gains an advantage when either the probability of contamination is high, or the contamination is uniform. This is likely due to the re-descending influence function of the Student's t-distribution — the smoother effectively throws out bad points rather than simply decreasing their impact to a certain threshold, as is the case for the  $\ell_1$ -smoother. As an example, results coming from a single run for the case where 50% of measurements are contaminated with the uniform distribution on  $[-10, 10]$  are displayed in Figure 6.1. Notice that T-Robust has an advantage over the  $\ell_1$ -smoother.

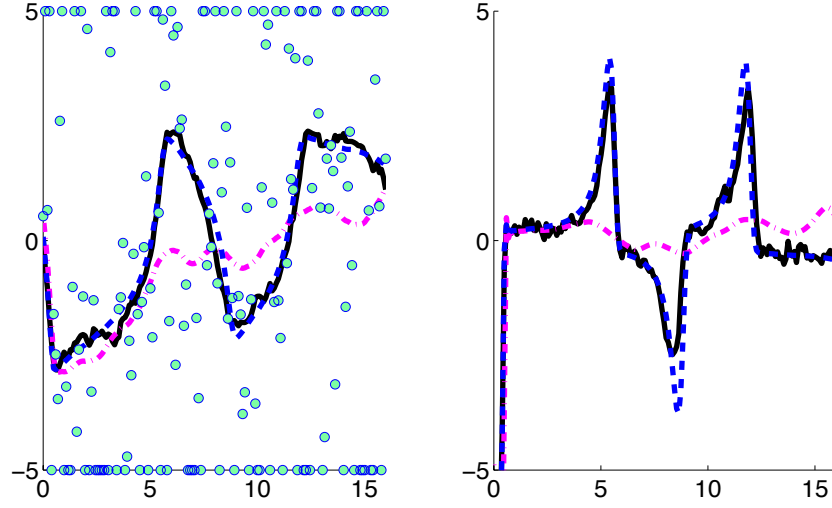


FIG. 6.2. Van Der Pol oscillator: smoother fits for X-component (left) and Y-component (right), with **70% outliers**  $N(0, 100)$ . Black solid line is truth, magenta dash-dot is the  $\ell_1$  smoother result, and blue dashed line is T-robust. Measurements on X-component are shown as dots, with outliers outside the range  $[-5, 5]$  plotted on top and bottom axes.

**6.2. T-Robust Smoother: Van Der Pol oscillator.** In this section, we present results for the Van Der Pol oscillator (VDP), described in detail in [2]. The VDP oscillator is a coupled nonlinear ODE defined by

$$\begin{aligned}\dot{x}_1(t) &= x_2(t) \\ \dot{x}_2(t) &= \mu[1 - x_1(t)^2]x_2(t) - x_1(t)\end{aligned}$$

The process model here is the Euler approximation for  $X(t_k)$  given  $X(t_{k-1})$ :

$$g_k(x_{k-1}) = \begin{pmatrix} x_{1,k-1} + x_{2,k-1}\Delta t \\ x_{2,k-1} + \{\mu[1 - x_{1,k-1}^2]x_{2,k-1} - x_{1,k-1}\}\Delta t \end{pmatrix}.$$

For this simulation, the *ground truth* is obtained from a stochastic Euler approximation of the VDP. To be specific, with  $\mu = 2$ ,  $N = 164$  and  $\Delta t = 16/N$ , the ground truth state vector  $x_k$  at time  $t_k = k\Delta t$  is given by  $x_0 = (0, -0.5)^T$  and for  $k = 1, \dots, N$ ,  $x_k = g_k(x_{k-1}) + w_k$ , where  $\{w_k\}$  is a realization of independent Gaussian noise with variance 0.01.

In [2], the  $\ell_1$ -Laplace smoother was shown to have superior performance to the  $\ell_2$ -smoother, both implemented in [1]. We compared the performance of the nonlinear T-robust and nonlinear  $\ell_1$ -Laplace smoothers, and found that T-robust gains an advantage in the extreme cases of 70% outliers. Figure 6.2 illustrates results coming from a single representative run. For 40% or fewer outliers, it is hard to differentiate the performance of the two smoothers for this nonlinear example.

**6.3. T-Robust Smoother: underwater Tracking Application.** This application is described in detail in [2], so we just give a brief overview here. In [2] we used the application to test the  $\ell_1$ -Laplace smoother. Here we use it for a qualitative



comparison between the T-Robust smoother, the  $\ell_1$ -Laplace smoother, and the  $\ell_2$  smoother with outlier removal.

In this experiment, a tracking target was hung on a steel cable approximately 200 meters below a ship. The pilot was attempting to keep the ship in place (hold station) at specific coordinates, but the ship was pitching and rolling due to wave action. The measurements for the smoother were sound travel times between the tracking target and four bottom mounted transponders at known locations, and pressure readings from a gauge that was placed on the target. Tracking data was independently verified using a GPS antenna mounted on a ship, and the GPS system provided sub-meter accuracy in position.

Pressure measurements in absolute bars were converted to depth in meters by the formula

$$\text{depth} = 9.9184(\text{pressure} - 1).$$

We use  $N$  to denote the total number of time points at which we have tracking data. For  $k = 1, \dots, N$ , the state vector at time  $t_k$  is defined by  $x_k = (e_k, n_k, d_k, \dot{e}_k, \dot{n}_k, \dot{d}_k)^T$  where  $(e_k, n_k, d_k)$  is the ( east, north, depth ) location of the object (in meters from the origin), and  $(\dot{e}_k, \dot{n}_k, \dot{d}_k)$  is the time derivative of this location.

The measurement vector at time  $t_k$  is denoted by  $z_k$ . The first four components of  $z_k$  are the range measurements to the corresponding bottom mounted transponders and the last component is the depth corresponding to the pressure measurement. For  $j = 1, \dots, 4$ , the model for the mean of the corresponding range measurements was

$$h_{j,k}(x_k) = \|(e_k, n_k, d_k) - b_j\|_2 - \Delta r_j.$$

These measurements were assumed independent with standard deviation 3 meters. These depth measurements were assumed to have standard deviation of 0.05 meters. We use  $\Delta t_k$  to denote  $t_{k+1} - t_k$ . The model for the mean of  $x_{k+1}$  given  $x_k$  was

$$g_{k+1}(x_k) = (e_k + \dot{e}_k \Delta t_k, n_k + \dot{n}_k \Delta t_k, d_k + \dot{d}_k \Delta t_k, \dot{e}_k, \dot{n}_k, \dot{d}_k)^T.$$

The process noise corresponding to east, north, and depth components of the conditional distribution of  $x_{k+1}$  given  $x_k$  was assumed to be Gaussian, with mean zero and standard deviation  $.01\Delta t_k$ . The process noise corresponding to the derivative vector of east, north, and depth components of the conditional mean  $x_{k+1}$  given  $x_k$  was also assumed Gaussian with mean zero and standard deviation  $.2\Delta t_k$ .

$\ell_2$ -smoother results without outlier removal are shown in Figure 6.3. There are three large peaks (two in the east component and one in the north component of the state) that are due to measurement outliers, and require either an outlier removal strategy or robust smoothing.

Three fits are shown in Figure 6.4:  $\ell_1$ -Laplace, T-Robust, and  $\ell_2$ -smoother with outlier removal. The darker curves appearing below the track are independent verifications using the GPS tracking near the top of the cable. A depth of 198 meters was added to the depth location of the GPS antenna so that the depth comparison can use the same axis for both the GPS data and the tracking results. Note that the time scale for the depth plots different (much finer) than the north, east, down plots, and demonstrates the accuracy of the GPS tracking as validated by the pressure sensor. T-Robust, like the  $\ell_1$ -Laplace smoother, was able to use the whole data sequence, despite large outliers in the data. The fits look very similar, and it is clear that

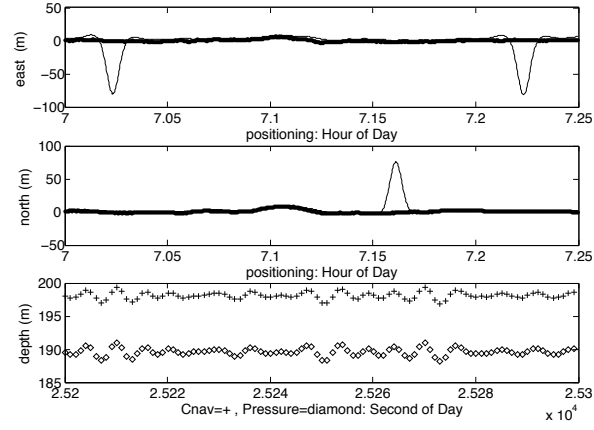


FIG. 6.3. *Track: Independent GPS verification (thick line and +),  $\ell_2$ -smoother estimate (thin line). Note the large outliers in the data.*

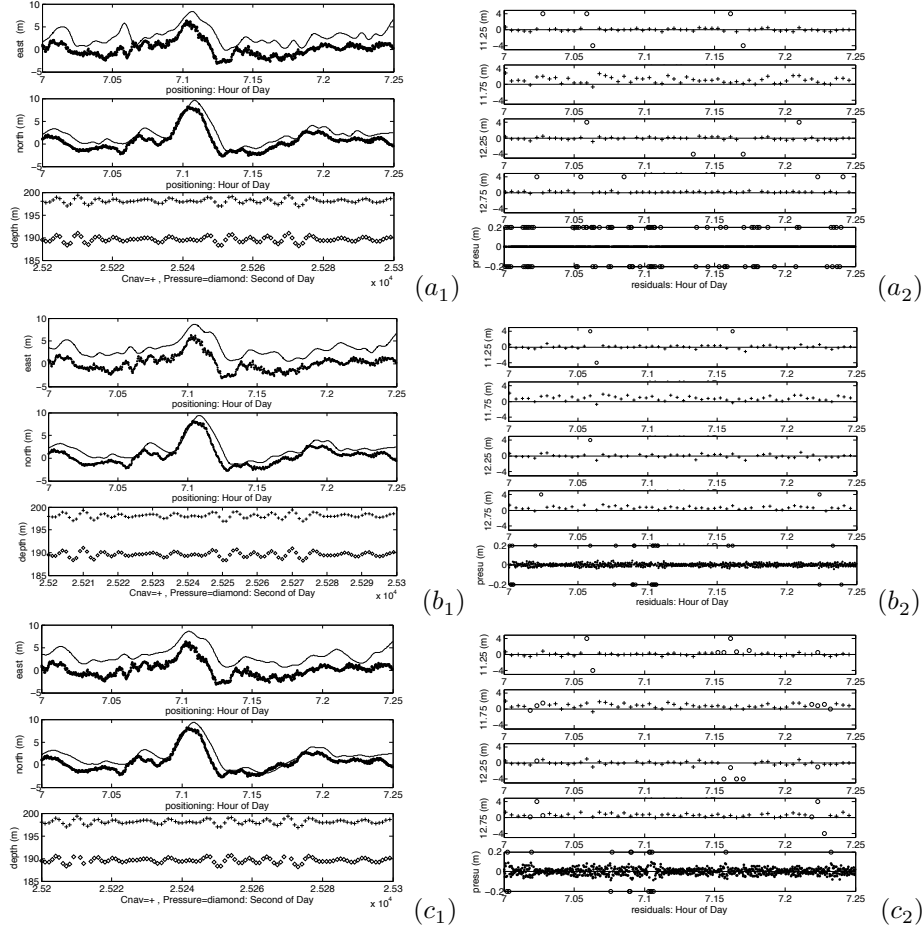


FIG. 6.4. *Track: Independent GPS verification (thick line and +) and Residuals for (a):  $\ell_1$ -Laplace smoother (thin line), (b): T-Robust smoother (thin line), (c):  $\ell_2$ -smoother with outlier removal.*

T-Robust can also be used for smoothing in the presence of outliers. Note that the T-Robust track (b) is smoother than the  $\ell_1$ -Laplace track (a) but has more detail than the  $\ell_2$ -smoother track with outlier removal (c). This is easiest to see by comparing the east coordinates in (a), (b), and (c) of Figure 6.4, between 7.2 and 7.25 hours.

The residual plots in Figure 6.4 are quite revealing. Outliers are defined as measurements corresponding to residuals with absolute value greater than three standard deviations from the mean. All outliers are shown as ‘o’ characters, and those that fall outside the axis limits are plotted on the vertical axis limit lines. Note that the  $\ell_2$ -smoother with outlier removal detects outliers after the first fit that are not outliers after the second fit. The peaks in Figure 6.3 are large enough to influence the entire fit, and so some points which are actually ‘good’ measurements are removed by the  $3\sigma$  edit rule, resulting in ‘over-smoothing’ of the outlier removal track and more detail in both of the robust smoothers in Figure 6.4.

The  $\ell_1$ -Laplace smoother pushes more of the residuals to zero, particularly those corresponding to depth measurements, which are the most reliable and frequent. The T-Robust smoother is somewhere in between — the residuals for the depth track are smaller in comparison to the residuals of the  $\ell_2$ -smoother, but are not set to zero as by the  $\ell_1$ -Laplace smoother. As discussed previously, these features are artifacts of the behavior of the distributions at zero, and the choice of smoother should be guided by particular applications.

#### 6.4. T-Trend Smoother: reconstruction of a sudden change in state.

We present a proof of concept result for the T-Trend smoother, using two Monte Carlo studies of 200 runs. In the first study, the state vector, as well as the process and measurement models, are the same as in Sec. 6.1. At any run,  $x_2$  has to be reconstructed from 20 measurements corrupted by a white Gaussian noise of variance 0.05 and collected on  $[0, 2\pi]$  using a uniform sampling grid. The top panel of Figure 6.5 reports the boxplot of the 200 root-MSE errors for the  $\ell_2$ -,  $\ell_1$ -, and T-Trend smoothers, while the top right panel of Figure 6.5 displays the estimate obtained in a single run. It is apparent that the performance of the three estimators is very similar.

The second experiment is identical to the first one except that we introduce a ‘jump’ at the middle of the sinusoidal wave. The bottom panel of Figure 6.5 reveals the superior performance of the T-Trend smoother under these perturbed conditions. The result depicted in the bottom right panel of Figure 6.5 for a single run of the experiment is representative of the average performance of the estimators. The estimate achieved by the  $\ell_2$ -smoother (dashed-line) does not follow the jump well (the true state is the solid line). The  $\ell_1$ -smoother (dashdot) does a better job than the  $\ell_2$ -smoother, and the T-trend smoother outperforms the  $\ell_1$ -smoother, following the jump very closely while still providing a good solution along the rest of the path.

**6.5. Reconstruction of a sudden change in state in the presence of outliers.** Until now, we have considered robust and trend applications separately, in order to compare with previous robust smoothing formulations and to highlight the main features of the trend-filtering problem. A natural extension is to consider these features in tandem — in other words, can we smooth a track which has *both* outliers and a sudden change in state? In fact, smoothers of this nature (but exploiting convex formulations) have already been proposed [14].

The challenge to building such a strong smoother is that without prior knowledge, it is difficult to tell the difference between a bad measurement (an outlier) and a good measurement that may be consistent with a sudden change in the state. In many cases, the user will be aware that some sensors are reliable, while others are subject to

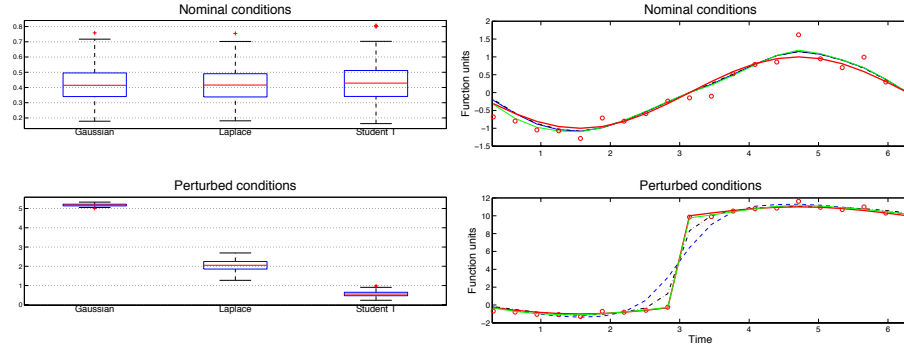


FIG. 6.5. Reconstruction of a sudden change in state obtained by  $\ell_2$ ,  $\ell_1$ , and  $T$ -Trend smoothers. **Left:** Boxplot of reconstruction errors under nominal (top) and perturbed (bottom) conditions. **Right:** Reconstructions obtained using  $\ell_2$  (dashed),  $\ell_1$  (dashdot) and  $T$ -Trend (thin line) smoother. The thick line is the true state.

contamination. This kind of prior information can now easily be incorporated using the generality and flexibility of section 3, so that the user may specify trustworthy sensors (by modeling corresponding residuals *indices* with Gaussians) as well as stable state components (by modeling corresponding innovation residual *indices* with Gaussians). Note that this is very different from specifying which of the individual *measurements* are reliable, or which individual *transitions* follow the process model.

In this section, we consider a situation where we have a trustworthy sensor  $s_1$  and an occasionally malfunctioning sensor  $s_2$ . Sensor  $s_2$  gives frequent measurements, but some proportion of the time is subject to heavy contamination, while sensor  $s_1$  gives measurements rarely, but they are trustworthy (i.e. only subject to small Gaussian noise). Using the flexible interface implemented in [1], we can model  $s_1$  errors as Gaussian and  $s_2$  errors as Student's  $t$ .

We use setup in section 6.4 together with the Gaussian outlier contamination scheme described in section 6.1. Both measurements are direct, so the measurement matrix in this case is

$$H_k x_k = \begin{bmatrix} 0 & 1 \\ 0 & 1 \end{bmatrix} x_k, \quad R_k = \begin{bmatrix} \sigma^2 & \\ & \sigma^2 \end{bmatrix}.$$

Since in the ckbs interface, the user specifies  $R_k^{-1}$  rather than  $R_k$ , missing measurements are easily specified by setting the corresponding component of  $R_k^{-1}$  to 0.

For the contaminated sensor  $s_2$ , we consider  $p = .2$  contamination level, and  $\phi = 100$ , very large contaminating variance. We have  $s_2$  measurements at every time step, but  $s_1$  measurements only at every 10th time step.

The results are shown in figure 6.6. Measurements are plotted using diamonds, with  $s_2$  measurements represented by small symbols, while  $s_1$  measurements are represented by large symbols. Ground truth is shown using a solid black line, and smoother results are shown using a red dashed line. Results in panel (a) were obtained using the least squares smoother, which cannot handle outliers. Results in panel (b) were obtained using T-Robust only, applying Student's  $t$  modeling only to the measurement components. The resulting fit is much better, but the smoother struggles to follow the jump in the track, overestimating the curve before the jump and underestimating it after the jump. Results in panel (c) were obtained by the Double T smoother, which modeled all residuals and innovations using Student's  $t$ . Double T

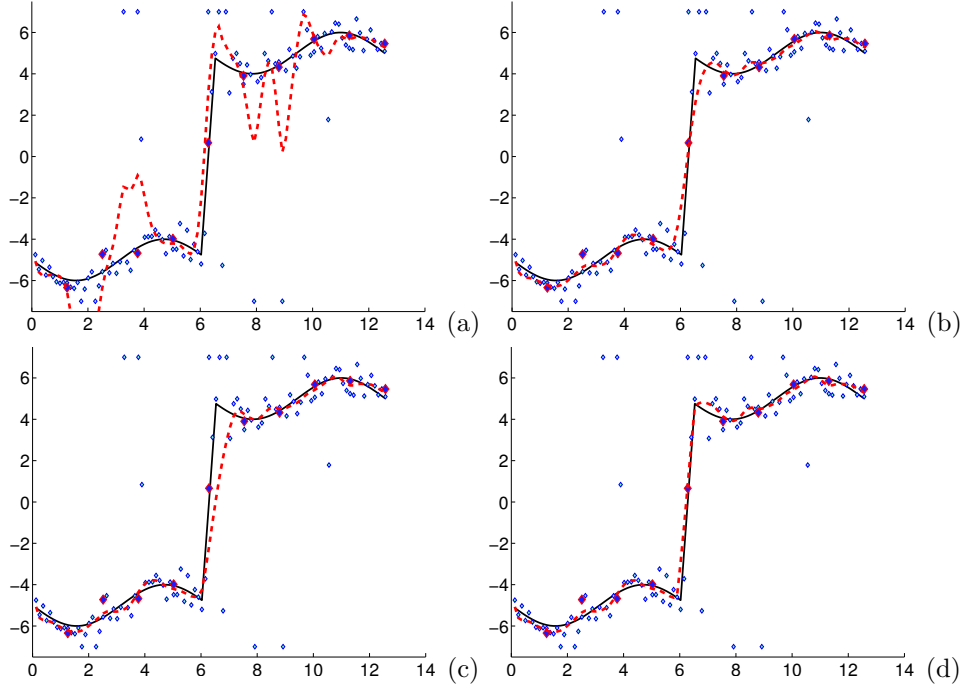


FIG. 6.6. Tracking a sudden change in the presence of outliers. Measurements are plotted using diamonds, with  $s_2$  measurements (frequent, contaminated) represented by small symbols, while  $s_1$  measurements (rare, reliable) represented by large symbols. Outliers appear on the axes when they are out of range of the plot limits. Ground truth is shown using a solid black line, and smoother results are shown using a red dashed line. (a): Least squares smoother (Gaussian errors for process and measurements) is very vulnerable to outliers. (b): T-Robust only (Gaussian errors for process components and  $s_1$ , Student's  $t$  errors for  $s_2$ ) effectively ignores the outliers, but struggles to follow sharp change in state. (c): Double T smoother (Student's  $t$  errors for all components): ignores outliers, but struggles to follow sudden change in state. (d): Trend following robust smoother (Student's  $t$  errors for process components and  $s_2$ ; Gaussian for  $s_1$ ): ignores outliers and follows sudden change in state, using information in the reliable measurements.

follows the curve well before the jump, but not after. Note that there are a couple of measurements sitting along the sharp jump — the Double T suspects these to be outliers, only trusting the concentrated measurements to the right of the jump.

Finally, results in panel (d) were obtained by using the information about which measurements are reliable. Specifically, Student's  $t$  modeling was used for all innovations residuals and for  $s_2$ , and Gaussian modeling was used for the  $s_1$  component. This smoother ignores the outliers and is able to follow the jump very well, since it takes advantage of the fact that there is a reliable measurement that happens to be sitting right in the middle of the transition.

The file used to generate the subplots in the figure is `noisy_jump_two_meas.m`, which can be accessed through the `example` subdirectory of [1].

**7. Discussion and Conclusions.** We have presented a generalized Student's  $t$  smoothing framework, which allows modeling any innovations or measurement residuals using Student's  $t$  errors, and includes T-Robust and T-Trend, and Double T smoothers as important special cases. All of the smoothers in the framework efficiently solve for the MAP estimates of the states in a state-space model with any selected set of

residuals modeled using Student’s t or Gaussian noise. We have shown that these features can be used independently and in tandem, work for linear and nonlinear process models, and can be used both for outlier-robust smoothing and for tracking sudden changes in the state.

Similar to contributions in other applications, e.g. sparse system identification [10, 27, 30], our results underscore the significant advantages of using heavy tailed distributions in statistical modeling. Heavy tailed distributions force the use of non-convex loss functions to solve for the associated MAP estimates [6, Theorem 2]. The consequent challenge is to optimize a non-convex objective even when the system dynamics are linear. In contrast to the convex case, this requires an iterative smoother. The convergence analysis for these methods is still developed within the general framework of convex-composite optimization [9], although the details of the analysis differ.

Because the problems are non-convex, iterative methods may converge to local rather than global minima. This problem can be mitigated by an appropriate initialization procedure—for example, in the presence of outliers, the  $\ell_1$ -Laplace smoother can be used to obtain a starting point for the optimizer, in which case we can improve on the  $\ell_1$  solution when the data is highly contaminated with outliers. This approach was not taken in our numerical experiments, which used the same initial points. For all the linear experiments, the initial point was simply the null state sequence. For the Van Der Pol, the initial state  $x_0$  was correctly specified in all experiments, and the remaining state estimates in the initial sequence were null.

The T-Robust smoother compares favourably to the  $\ell_1$ -Laplace smoother described in [2], and outperforms it in our experiments when the data is heavily contaminated by outliers. The T-Trend smoother was designed for tracking signals that may exhibit sudden changes, and therefore has many potential applications in areas such as navigation and financial trend tracking. It was demonstrated to follow a fast jump in the state better than a smoother with a convex penalty on model deviation. Finally, we demonstrated the power of a new method by tracking a fast change in the presence of outliers using the full flexibility of the presented framework, which allowed us to differentially model residuals for sensors which we knew to be reliable vs. unreliable, and to design a smoother that was robust to outliers yet able to track sudden changes.

An important question in the design and implementation of Student’s t-based smoothers is how to estimate the degree of freedom parameter  $\nu$ . In all of our experiments, we have treated this parameter as fixed and known. We note that there are established EM-based methods in the literature for estimating these parameters [13, 19], as well as recently proposed methods [7], and we leave the implementation of these extensions in the Kalman smoothing framework to future work.

**8. Acknowledgements.** The authors would like to thank Bradley Bell and North Pacific Acoustic Laboratory (NPAL) investigators of the Applied Physics Laboratory, University of Washington for the underwater tracking data used in this paper (NPAL is sponsored by the Office of Naval Research code 321OA). We are also grateful to Michael Gelbart for insightful discussions about the numerical experiments.

## REFERENCES

- [1] A.Y. Aravkin, B.M. Bell, J.V. Burke, and G. Pillonetto. CKBS: Matlab/Octave package for constrained and robust Kalman smoothing. <http://www.coin-or.org/CoinBazaar/ckbs/ckbs.xml>, 2007-2013.

- [2] A.Y. Aravkin, B.M. Bell, J.V. Burke, and G. Pillonetto. An  $\ell_1$ -Laplace robust Kalman smoother. *IEEE Transactions on Automatic Control*, 2011.
- [3] A.Y. Aravkin, B.M. Bell, J.V. Burke, and G. Pillonetto. Learning using state space kernel machines. In *Proc. IFAC World Congress 2011*, Milan, Italy, 2011.
- [4] A.Y. Aravkin, B.M. Bell, J.V. Burke, and G. Pillonetto. New stability results and algorithms for block tridiagonal systems, with applications to kalman smoothing. <http://arxiv.org/abs/1303.5237>, 2013.
- [5] A.Y. Aravkin, J.V. Burke, and G. Pillonetto. Robust and trend following kalman smoothers using student's t. In *Proc. of SYSID*, 2012.
- [6] A.Y. Aravkin, M.P. Friedlander, F. Herrmann, and T. van Leeuwen. Robust inversion, dimensionality reduction, and randomized sampling. *Mathematical Programming*, 134(1):101–125, 2012.
- [7] A.Y. Aravkin and T. van Leeuwen. Estimating nuisance parameters in inverse problems. *Inverse Problems*, 28(11):115016, 2012.
- [8] B. M. Bell, J. V. Burke, and G. Pillonetto. An inequality constrained nonlinear Kalman-Bucy smoother by interior point likelihood maximization. *Automatica*, 2008.
- [9] J.V. Burke. Descent methods for composite nondifferentiable optimization problems. *Mathematical Programming*, 33:260–279, 1985.
- [10] A. Chiuso and G. Pillonetto. Learning sparse dynamic linear systems using stable spline kernels and exponential hyperpriors. In *In Advances in Neural Information Processing Systems (NIPS)*, 2010.
- [11] Charles Chui and Guanrong Chen. *Kalman Filtering*. Springer, 2009.
- [12] L. Fahrmeir and H. Kaufmann. On Kalman filtering, posterior mode estimation, and Fisher scoring in dynamic exponential family regression. *Metrika*, pages 37–60, 1991.
- [13] Ludwig Fahrmeir and Rita Kunstler. Penalized likelihood smoothing in robust state space models. *Metrika*, 49:173–191, 1998.
- [14] S. Farahmand, G.B. Giannakis, and D. Angelosante. Doubly robust smoothing of dynamical processes via outlier sparsity constraints. *Signal Processing, IEEE Transactions on*, 59(10):4529–4543, oct. 2011.
- [15] A. Gelb. *Applied Optimal Estimation*. The M.I.T. Press, Cambridge, MA, 1974.
- [16] Frank R. Hampel, Elvezio M. Ronchetti, Peter J. Rousseeuw, and Werner A. Stahel. *Robust Statistics: The Approach Based on Influence Functions*. Wiley Series in Probability and Statistics, 1986.
- [17] T. J. Hastie, R. J. Tibshirani, and J. Friedman. *The Elements of Statistical Learning. Data Mining, Inference and Prediction*. Springer, Canada, 2001.
- [18] R. E. Kalman. A new approach to linear filtering and prediction problems. *Transactions of the AMSE - Journal of Basic Engineering*, 82(D):35–45, 1960.
- [19] Kenneth L. Lange, Roderick J. A. Little, and Jeremy M. G. Taylor. Robust statistical modeling using the t distribution. *Journal of the American Statistical Association*, 84(408):881–896, 1989.
- [20] Ricardo A. Maronna, Douglas Martin, and Yohai. *Robust Statistics*. Wiley Series in Probability and Statistics. Wiley, 2006.
- [21] H. Ohlsson, F. Gustafsson, L. Ljung, and S. Boyd. State smoothing by sum-of-norms regularization. *Automatica (to appear)*, 2011.
- [22] R. T. Rockafellar. *Convex Analysis*. Princeton University Press, 1970.
- [23] R.T. Rockafellar and R.J.B. Wets. *Variational Analysis*, volume 317. Springer, 1998.
- [24] I.C. Schick and S.K. Mitter. Robust recursive estimation in the presence of heavy-tailed observation noise. *The Annals of Statistics*, 22(2):1045–1080, June 1994.
- [25] J.C. Spall. Estimation via Markov chain Monte Carlo. *Control Systems Magazine, IEEE*, 23(2):34 – 45, April 2003.
- [26] R. Tibshirani. Regression shrinkage and selection via the LASSO. *Journal of the Royal Statistical Society, Series B.*, 58, 1996.
- [27] M. Tipping. Sparse bayesian learning and the relevance vector machine. *Journal of Machine Learning Research*, 1:211–244, 2001.
- [28] G. Wahba. *Spline models for observational data*. SIAM, Philadelphia, 1990.
- [29] Mike West and Jeff Harrison. *Bayesian Forecasting and Dynamic Models*. Springer, second edition, 1999.
- [30] D.P. Wipf and B.D. Rao. An empirical bayesian strategy for solving the simultaneous sparse approximation problem. *IEEE Transactions on Signal Processing*, 55(7):3704–3716, 2007.
- [31] S.J. Wright. Solution of discrete-time optimal control problems on parallel computers. *Parallel Computing*, 16:221–238, 1990.